Grain scale processes recorded by oxygen isotopes in olivine-hosted melt inclusions from two MORB samples

Mélina Manzini, Anne-Sophie Bouvier, Lukas Baumgartner, Estelle F. Rose-Koga, Pierre Schiano, Nobumichi Shimizu

Grain scale processes recorded by oxygen isotopes in olivine-hosted melt inclusions from two MORB samples

Mélina Manzini[1], Anne-Sophie Bouvier[1*], Lukas P. Baumgartner[1], Estelle F. Rose-Koga[2], Pierre Schiano[2], Nobumichi Shimizu[3]

[1] Institute of Earth Sciences, University of Lausanne, 1015 Lausanne, Switzerland

(melina.manzini@gmail.com; anne-sophie.bouvier@unil.ch; lukas.baumgartner@unil.ch)

[2] Laboratoire Magmas et Volcans, University of Blaise Pascal-CNRS-IRD, Clermont-Ferrand, France

(estelle.koga@uca.fr; p.schiano@opgc.fr)

[3] Woods Hole Oceanic Institution, Woods Hole, MA 02543, USA

(nshimizu@whoi.edu)

Corresponding author: A.-S. Bouvier (anne-sophie.bouvier@unil.ch)

Abstract

Although olivine-hosted melt inclusions from mid ocean ridge basalts (MORB) are commonly used as a proxy for mantle composition, these melt inclusions generally show larger elemental and isotopic compositional variation than their host lavas and the origin of these heterogeneities remains disputed. Here we present oxygen isotope data from melt inclusions hosted in olivine from two samples from the Mid-Atlantic ridge. Melt inclusions from different crystals within the same sample show more than 2.5‰ $\delta^{18}O$ variation within

each sample, which is nearly eight times the analytical error of 0.3‰ (2 standard deviations) and five times the $\delta^{18}O$ range in unaltered MORB. Measured $\delta^{18}O$ in melt inclusions do not correlate with common magmatic tracers, and $\delta^{18}O$ measured in the host olivines suggest a maximum of 1‰ $\delta^{18}O$ source heterogeneity. Less than half of the melt inclusions from each sample are in equilibrium with their host crystals; the remaining melt inclusions have either lower or higher olivine-melt oxygen isotope partition coefficients compared to the theoretical equilibrium values. Here we discuss several potential processes that could contribute to these observations, but none satisfactorily explain the olivine-melt inclusion oxygen disequilibrium that we observe in these samples. Nevertheless, it seems clear that the variability of $\delta^{18}O$ in melt inclusion from two MORB samples do not record only common magmatic process(es), but rather a localized grain scale process. Any $\delta^{18}O$ variation in melt inclusions should thus be interpreted with caution.

Keywords

Olivine-hosted melt inclusions; MORB; Mid-Atlantic Ridge; oxygen isotopes; grain scale processes; heterogeneity; SIMS

Introduction

Olivine-hosted melt inclusions are often used to study the origin and evolution of mantle-derived magmas (for a review, see Kent, 2008; Schiano, 2003 and references therein). Melt inclusions are physically isolated from their host magma, which undergoes different processes during magmatic evolution after the entrapment of melt inclusions (for example, magma mixing, assimilation, degassing). An important observation is that larger elemental and

46 isotopic compositional variations are generally observed in melt inclusions when compared to
47 whole-rock or glass compositions. A widespread interpretation is that variations measured in
48 melt inclusions reflect magmatic diversity that is not recorded in whole rock compositions
49 due to obscuration during later processes (e.g., Kent, 2008). In some cases, variations could
50 also be related to small-scale reactions in the melt in which the olivine is growing
51 (Danyushevsky et al., 2004).

52 In mid-oceanic ridge basalts (MORB), most melt inclusions have trace-element compositions
53 in the range of MORB lavas, but there are also some clear exceptions to this general
54 observation (see Schiano, 2003 for a review). These 'anomalous' trace-element compositions
55 have usually been interpreted to reflect near-fractional melting of a depleted mantle and/or
56 spinel lherzolite, or of hydrothermally altered peridotite (e.g., Gurenko and Chaussidon, 1995;
57 Nielsen et al., 2000; Sobolev and Shimizu, 1993). The anomalous trace-element compositions
58 are not found in MORB rocks, as MORBs represent aggregates of different melt fractions
59 (e.g., Jin et al., 1994; McKenzie, 1984; Sobolev and Shimizu, 1993). Melt reaction within the
60 crust, i.e. within a crystal mush, may also explain the larger compositional variations
61 observed in some MORB melt inclusions compared to lavas (e.g., Danyushevsky et al., 2004;
62 Kamenetsky and Gurenko, 2007).

63 Major and trace element variability in melt inclusions from MORB samples are also
64 sometimes observed within a single phenocryst (Shimizu, 1998), which indicates that melt
65 inclusions are not necessarily in equilibrium with their hosts. Such small-scale diversity could
66 be generated by trace element diffusion within the melt during melt inclusion formation by
67 host dissolution-reprecipitation, or by boundary layer entrapment during fast, diffusion-
68 controlled growth or melt transport (e.g., Baker, 2008; Cottrell et al., 2002; Faure and
69 Schiano, 2005; Manzini et al., 2017; Van Orman et al., 2002). Other processes, such as
70 diffusion of some elements (e.g., H, Fe) toward the host olivine or the host melt are

responsible, in some cases, for elemental variation in melt inclusions (e.g., Danyushevsky et al., 2000a; Gaetani et al., 2012).

To date, no stable isotope data from melt inclusions within olivine from typical MORB samples have been published. Although $\delta^{11}B$ and $\delta^{18}O$ were reported in some olivine-hosted melt inclusions from Iceland, the petrogenetic history of these samples is fundamentally different from typical MORB settings (Gurenko and Chaussidon, 1997, 2002; Hartley et al., 2013). In this study, we focus on $\delta^{18}O$ values from melt inclusions within MORB samples, as the systematics of this stable isotope system are well constrained. Based on a compilation of $\delta^{18}O$ data in Neogene volcanic rocks, Harmond and Hoefs (1995) concluded that bulk MORB rocks have $\delta^{18}O$ compositions of 5.7‰ ± 0.2‰. Because the variation reported is similar to the typical analytical uncertainty reported in the literature for individual $\delta^{18}O$ measurements of silicate rocks at that time, the authors concluded that MORB have a uniform $\delta^{18}O$ signature. More recently, fresh MORB glasses from the Mid-Atlantic Ridge, Indian Ocean and east Pacific Ridge were analyzed by laser fluorination and show a narrow range of oxygen isotope ratios from 5.37 ± 0.01 to 5.81 ± 0.04 ‰ (1σ), with an average of +5.50 ‰ (Eiler et al., 2000). In addition, $\delta^{18}O$ is thought to not fractionate during melting (e.g., Eiler, 2001). As such, if melt inclusions are representative of the MORB source, they should show similar values within a relatively restricted range; however, as melt inclusions generally show larger chemical variations than those recorded by the bulk rock, $\delta^{18}O$ in melt inclusions from MORB samples might also display larger isotopic variabilities than MORB glasses. Constraining the variability of oxygen isotopes in melt inclusions from MORB samples is important, as $\delta^{18}O$ variations within these melt inclusions serve to assess the importance of fluid interaction, magma mixing and/or assimilation of oceanic crust (Gurenko and Chaussidon, 2002; Hartley et al., 2013). In this study we report $\delta^{18}O$ data from melt inclusions within two different MORB samples from the northern Mid-Atlantic Ridge. We observe a

never before reported large range of $\delta^{18}O$ compositions within these melt inclusions, up to 2.5‰, and discuss the reported data in term of magmatic processes, olivine dissolution-precipitation and diffusion.

Sample description and geological context

The studied olivine-hosted melt inclusions are from two dredged basalts from the North Atlantic ridge. Sample ARP73-10-03 is a picrite from the FAMOUS zone (36°8372'N, 33°2482'W) that contains a little more than 20% olivine phenocrysts ($Fo_{87.2-91.3}$), rare clinopyroxene, and plagioclase xenocrysts. The crystals are surrounded by a hyalocrystalline groundmass composed of glass, plagioclase (An_{75-80}) and olivine microlites (Fo_{86}) (Laubier et al., 2007). Laubier et al. (2007) suggest that the variable major and trace element compositions of ARP73-10-03 melt inclusions reflect polybaric partial melting of a homogeneous mantle, followed by mixing in various proportions at either different degrees of melting or in different parts of the melting system.

CH77-DR6-203 is a dredged basalt from the 14° MAR triple junction (14.12°N, 45°W). This fresh sample is highly enriched in volatiles, with CO_2 in vesicles and water in the glass, (popping rock; Javoy and Pineau, 1991) and shows a compositional anomaly with enriched $(Nb/Zr)_N$, $(Ta/Hf)_N$ and $(La/Sm)_N$ compared to adjacent segments which may result from mantle heterogeneity (Bougault et al., 1988). The mantle heterogeneity hypothesis is also supported by Sr and Nd isotopes in MORB rocks from different segments of the triple junction (Dosso and Bougault, 1986). The melt inclusions studied here are hosted in 1-5 mm, polyhedral olivines containing one or several melt inclusions. They are glassy, sub-spherical, and have a radius of 40-350 μm. They contain no daughter minerals. Rare shrinkage bubbles are present, but represent only a small fraction of the total volume.

120

121 Methods

122

123 *Sample preparation*

124 Polished olivines containing exposed melt inclusions were pressed into 1-inch indium mounts,
125 along with the glass standards (BHVO-2G, BCR-2G and BIR-1G) and San Carlos olivine.
126 Care was taken to mount them within 8 mm of the center of the mount. A separate mount was
127 made for each sample. SEM images were acquired at the University of Lausanne using a
128 Tescan Mira LMU field-emission scanning electron microscope operated at 20 kV and 0.2-0.4
129 nA probe current to ensure that the melt inclusions were totally glassy. Melt inclusions with
130 cracks or crystals were discarded. Topography of each mount was measured using a Brucker
131 GTA-K white light interferometer.

132

133 *Electron microprobe*

134 Major element compositions and X-ray distribution maps of melt inclusions and olivines were
135 acquired using a JEOL 8200 Superprobe electron microprobe analyzer. Analytical conditions
136 for the quantitative measurement of olivine were 15kV at 20nA and a 5 μm beam diameter.
137 Counting times were 30 s for Si, Mg, Mn and Fe and 40 s for Al, Ca, Ni and Cr. Analytical
138 conditions for analyses of melt inclusions were 15kV, 10 nA and a 10 μm beam diameter.
139 Counting times were 30 s for all elements except for K (20 s) and Na (16 s). A glass standard
140 (KL2-G) was used for SiO_2 and Al_2O_3. All other elements were calibrated on minerals. A
141 grain of ML3B-G was used as an internal standard to check the calibration.

142

143 ***Secondary ion mass spectrometer***

144 Oxygen isotope ratios, volatiles (H_2O, CO_2, Cl, F) and trace-element (Ti, V, Sr, Y, Nb, Ba,
145 La, Ce, Nd, Sm, Eu, Yb) concentrations were determined using the CAMECA ims1280-HR at
146 the SwissSIMS laboratory.

147 *Oxygen isotopes*

148 Analytical conditions were similar to those described by Seitz et al. (2017): Throughout
149 $^{18}O/^{16}O$ measurements of melt inclusions and olivines, the sample was sputtered with a Cs^+
150 primary beam of 2 nA, which was raster over 15 μm. An electron gun was utilized in order to
151 compensate for sample charging. Samples were pre-sputtered for 30 s, followed by 80 s of
152 analysis (20 cycles of 4 s). Automatic centering of secondary ions on field and contrast
153 apertures were performed before each analysis. Measurements of ^{16}O and ^{18}O were performed
154 simultaneously via two Faraday cups, using 10^{10} and 10^{11} resistors, respectively. The intensity
155 of ^{16}O was typically ~ $2.2x10^9$ counts per second for glasses and ~$1.7x10^9$ counts per second
156 for olivine. Internal error (2 standard error), reflecting the counting statistics of one analysis,
157 was usually better than 0.3‰ for melt inclusions and olivines.

158 For melt inclusions, instrumental mass fractionation (IMF) was corrected using a set of 9
159 international glass standards with compositions ranging from basaltic to rhyolitic (NKT-1G,
160 GOR132-2G, BIR-2G, BHVO-2G, ML3B-2G, BCR-2G, StHs6/80G, UoE-Lipari, ATHO-G;
161 Hartley et al., 2012; Jochum et al., 2006). The matrix effect was corrected using a linear
162 regression of IMF with SiO_2 (Figure DR1-A). Two to three standards (BHVO, BIR and BCR),
163 with compositions closely bracketing the melt inclusion compositions, were added on each
164 mount to monitor and correct for potential instrumental drift. For olivines, IMF was corrected
165 using an in-house San Carlos olivine standard (Fo 90.1), as well as three in-house olivine
166 reference materials (Fo 99.6, Fo 91.9 and Fo 37.5; Fig DR1-B).

At the outset of each session, we performed at least eight measurements of a running standard (i.e., measured repeatedly during the session; BHVO for melt inclusions sessions and San Carlos for olivine sessions), in order to determine standard reproducibility (noted hereafter in 2 standard deviation, 2SD). The 2 SDs were better than 0.3‰ for melt inclusions sessions, and 0.4‰ for olivines sessions. To monitor the instrument stability, running standards were measured every 8 to 12 unknowns and gave a reproducibility of 0.3‰ 2SD, similar to the eight measurements at the outset of each session. Accuracy was checked using one of the two to three standards inserted in each mounts and was similar to reproducibility (0.3‰ 2SD and 0.4‰ 2SD for melt inclusions and olivines, respectively).

Trace elements

Phosphorous concentrations within melt inclusions were measured using the same analytical conditions described by Manzini et al. (2017): Trace-element compositions of melt inclusions and olivine were analyzed using a 5-6 nA O^- primary ion beam, resulting in an analysis spot of about 20 µm. A mass resolution of 5000 was used. Samples were pre-sputtered for 90 s, using a 25 µm raster. Trace elements were quantified by measuring the signal from the following isotopes: ^{48}Ti, ^{51}V, ^{88}Sr, ^{89}Y, ^{93}Nb, ^{138}Ba, ^{139}La, ^{140}Ce, ^{142}Nd, ^{152}Sm, ^{153}Eu, ^{172}Yb. These measurements were performed in mono-collection mode by peak switching throughout one analytical run on an electron multiplier (EM) collector. ^{40}Ca was measured on a FC collector in the same analytical run as the other trace elements and was used as reference element. Using ^{40}Ca instead of ^{30}Si (or ^{28}Si) during melt inclusion analyses allowed us to check for possible contamination by olivine throughout the analyses. A waiting time was used to obtain a steady state sputtering condition, and each analysis consisted of six cycles. Waiting and counting time, typical standard reproducibility and typical internal error are

191 given in Table DR1. BHVO-2G was used as standard for melt inclusions, using the USGS
192 certified values for the trace elements.

193

194 *Volatile elements*

195 A Cs^+ primary ion beam with a current of 1.5 nA was used to measure volatile elements
196 (H_2O, CO_2, Cl, F, S); throughout these analyses an electron gun was used to compensate the
197 charges and to avoid charging of the sample surface. The secondary beam was accelerated at
198 10 kV, and the sample was pre-sputtered applying a 15 μm raster for 210 s. Elements were
199 measured in mono-collection mode, with a 10 μm raster during 12 cycles. Total analysis time,
200 including pre-sputtering, was approximately 14 minutes. The field aperture was set to 3000
201 μm, entrance slit to 60 μm and exit slit to 240 μm. This configuration allowed a mass
202 resolution of 5000, sufficient to fully discriminate the interferences. BHVO-2G, BCR-2G,
203 BIR-1G, ALL, NS and ALV (Helo et al., 2011) were used as standards. BHVO-2G was then
204 used as a running standard to check instrument stability. Background was determined by
205 analysis of a synthetic anhydrous olivine. Additional information is given in Table DR1.

206

207 **Results**

208 A total of 34 melt inclusions within 30 olivines were measured from sample CH77-DR6-203,
209 as were 17 melt inclusions within 13 olivines from sample ARP73-10-03. The results of these
210 analyses are summarized in Table DR2. Oxygen isotope ratios in olivines are reported in
211 Table DR3.

212 Analyzed olivines are characterized by a high forsterite content (Fo = Mg/Fe+Mg) ranging
213 from 88.8 to 91.4 for ARP73-10-03 and from 84.0 to 90.9 for CH77-DR6-203. Major-element
214 compositions of melt inclusions were corrected for the effect of post-entrapment

crystallization (PEC) of olivine at the wall of melt inclusion, using the Petrolog software package (Danyushevsky and Plechov, 2011). Parameters used for Petrolog calculations are summarized in the footnote of Table DR2. Our calculated PEC indicates that between 5.9 and 18.1% of olivine crystallized after melt inclusion trapping. Major elements are less variable after PEC correction (e.g., SiO_2 variation of 2.8 wt. % before and 1.6 wt. % after correction; Table DR2), and all major-element compositions mentioned hereafter are corrected for PEC. Melt inclusions from ARP73-10-03 have a narrow range of major-element compositions, with SiO_2 ranging from 50.0-50.4 wt. %, MgO from 11.2-12.8 wt. % and K_2O from 0.10-0.15 wt. %. CH77-DR6-203 shows a slightly larger compositional range in major elements, with SiO_2 content from 49.2-50.8 wt. %, MgO from 7.8-10.0 wt. %, and K_2O from 0.20-0.55 wt % (Figure 1A). Major-, volatile- (Cl, F, S) and trace-element concentrations measured in ARP73-10-03 fall within the same range as those reported by Laubier et al. (2012) for melt inclusions within the same sample and are consistent with glass N-MORB compositions (Jambon et al., 1995; Naumov et al., 2014; Wallace and Carmichael, 1992). Water and CO_2 concentrations are also in the typical range of MORB glass values (Danyushevsky et al., 2000b; Magenheim et al., 1995; Wallace and Carmichael, 1992). The melt inclusions from CH77-DR6-203 are enriched in volatiles (to a lower extent for CO_2) when compared with MORB glass values, and have trace-element compositions similar to typical E-MORB glasses (e.g., Figure 1B modified from Gale et al., 2013).

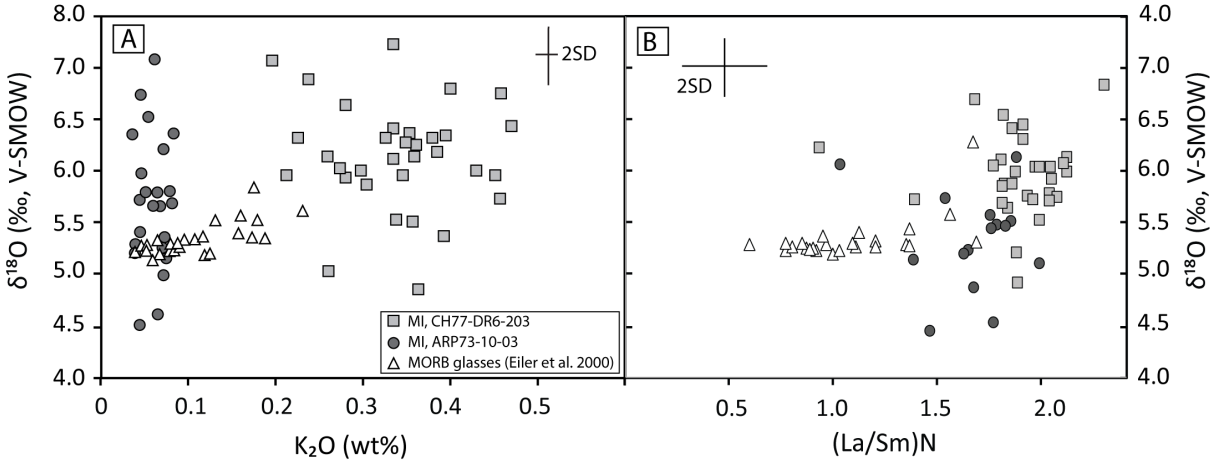

234

235 **Figure 1**: Oxygen isotope values for MI plotted against the K_2O concentration (A) and the La/Sm
236 chondrite-normalized ratio (McDonough and Sun, 1995) (B). Line separating D-, N- and E-MORB are
237 from Gale et al., 2013a. Fresh MORB glasses studied represented by white triangles in the figure, are
238 plotted for comparison (Eiler et al., 2000).

239

240 Oxygen isotopes from melt inclusions show > 2.3‰ variation within each sample ($\delta^{18}O$ =
241 +5.0 ± 0.17 to+7.2 ± 0.16‰, with an average of +6.2‰ for CH77-DR6-203; and $\delta^{18}O$ = +4.5
242 ± 0.3 to +7.1 ± 0.6‰, average +5.7‰ for ARP73-10-03). These variations are about eight
243 times larger than the analytical uncertainty (0.3‰, 2SD) and about five times larger than the
244 variations observed for bulk $\delta^{18}O$ of unaltered MORB glasses (<0.5‰; Figure 2). Before IMF
245 correction, data show similar $\delta^{18}O$ variations (2.2‰). This is explained by the relatively
246 narrow range of SiO_2 of the melt inclusions within a sample, which indicates that the applied
247 IMFs are relatively similar (± 0.13‰) for all melt inclusions from the same sample. ARP73-
248 10-03 is the closest to MORB glass composition in term of major, trace elements and oxygen
249 isotopes. Nevertheless, 8 melt inclusions out of 21 have 'anomalous' $\delta^{18}O$ composition (i.e.,
250 statistically – 2 SD – outside the range of MORB glass bulk values). Within a single olivine,
251 $\delta^{18}O$ from different melt inclusions are statistically different in the ARP73-10-03 sample (3
252 pairs, variation up to 2.2‰), whereas in the CH77-DR6-203 sample, melt inclusions hosted in

253 a single olivine have values within analytical uncertainty $\delta^{18}O$ (3 pairs, variation less than
254 0.4‰; Figure 3). In both samples, olivines show smaller variability than their hosted melt
255 inclusions: the ARP73-10-03 olivine have $\delta^{18}O$ values of +4.9 to +5.7‰ and olivines from
256 CH77-DR6-203 have $\delta^{18}O$ ranging from +5.0 to +6.5‰ (Table DR3, Figure 2).

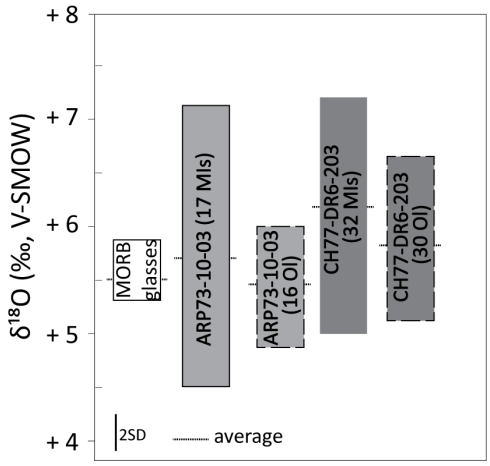

257

258 **Figure 2**: Comparison of oxygen isotope variations in MORB glasses from Mid-Atlantic Ridge,
259 Indian ocean and east-Pacific Ridge (n = 28) (Eiler et al., 2000) and melt inclusions (MIs) from the
260 two studied MORB samples (ARP73-10-03 and CH77-DR6-203). For a comparison, range of $\delta^{18}O$
261 composition measured in the olivines hosting the melt inclusions are also plotted (dashed line
262 contoured fields). Melt inclusions show larger variability compare to MORB glasses and to their host
263 olivines.

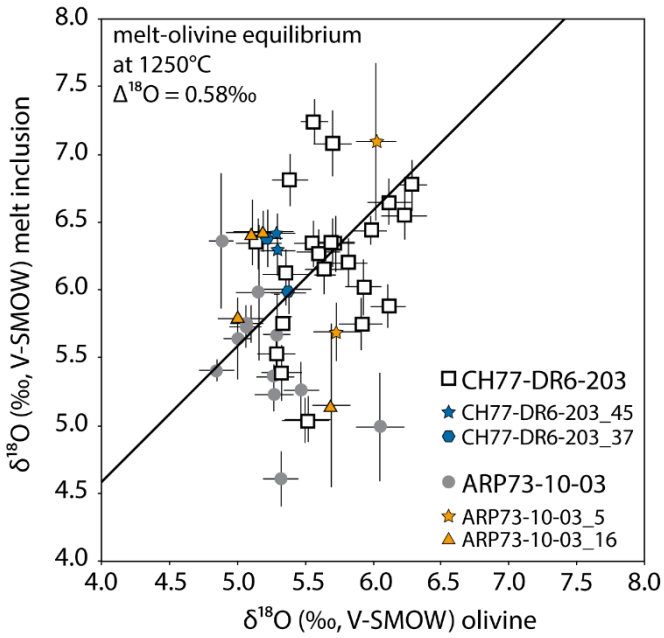

264

265 **Figure 3**: Oxygen isotope ratio of melt inclusions, compared to the $\delta^{18}O$ of their host olivine crystals.
266 Melt-olivine equilibrium fractionation ($\Delta^{18}O$; black line) is from Matthews et al. (1998). Only 42 and
267 46% of melt inclusions from ARP_73-10-03 and CH77-203-DR6 are in equilibrium with their host,
268 within analytical error.

269

270 ## Discussion

271 To date, no oxygen isotope data have been reported for olivine-hosted melt inclusions from
272 MORB samples. Only two studies (Gurenko and Chaussidon, 2002; Hartley et al., 2013)
273 reported $\delta^{18}O$ in olivine-hosted melt inclusions, and these data are from 7 samples taken from
274 Iceland. These studies found $\delta^{18}O$ variation reaching a maximum of 1.2 ‰ (+4.0 to +5.2‰,
275 sample 14161G, n = 3 melt inclusions; Gurenko and Chaussidon, 2002) and 0.95 ‰ (+3.05 to
276 +4.0‰, sample N18, n = 9 melt inclusions; Hartley et al., 2013), respectively. These
277 variations were interpreted to reflect either mixing of the ascending magma with melt lenses
278 that had previously interacted with the low-$\delta^{18}O$ Icelandic crust (Hartley et al., 2013), or
279 heterogeneity in the Icelandic mantle or mixing of two end-members (Gurenko and

280 Chaussidon, 2002). Melt inclusions from the two MORB samples measured in our study both
281 show more than 2.3‰ variation in $\delta^{18}O$, a larger variation than that reported for olivine-
282 hosted melt inclusions from Iceland. Hereafter, the $\delta^{18}O$ variability is discussed in term of
283 analytical versus magmatic processes.

284

285 *Analytical artefacts*

286 Oxygen isotope analyses via SIMS are very sensitive to the sample geometry, i.e. the
287 placement of the analyzed grains in the mount and the topography of the analyzed material
288 (e.g., Kita et al., 2009). All grains and reference material have been placed within 8 mm of the
289 center of the mount, in order to avoid X-Y effects due to deformation of the electrostatic field
290 close to the edge of the sample holder (Peres et al., 2013) (see methods section for more
291 details). Reproducibility of the measurements of a homogeneous reference material for
292 oxygen isotope is typically <0.3‰ (2 SD) when the surface relief is 1 µm, whereas it
293 increases up to 3‰ (2SD) when topography is on the order of 10-40 µm (Kita et al., 2009).
294 Our mounts show < 4 µm topography both between the indium and grains, and between
295 olivine and melt inclusions. Two different cases are presented in Figure 4: First, Figure 4-A
296 shows olivine CH77-DR6-203_37 hosting 2 melt inclusions with similar $\delta^{18}O$ (within the
297 0.3‰ 2SD calculated for a session, +6.37±0.21‰ and +5.97±0.16‰) and a topography of
298 1µm. Olivine ARP73-10-03_16, shown in Figure 4-B, has $\delta^{18}O$ in melt inclusions which vary
299 from +5.15 ± 0.21‰ to +6.42 ± 0.26‰. This olivine has a topographical variation of up to 4
300 µm, with a difference in topography of 1.5 µm between melt inclusions A, C and D
301 (maximum 1.3‰ difference in $\delta^{18}O$), and 2.5 µm between melt inclusions A and B (similar
302 $\delta^{18}O$). Melt inclusions are less than 1 µm lower compared to the olivine, which should not
303 affect the analyses: 17 analyses made following 2 profiles along perpendicular axes from wall

304 to wall in melt inclusion A, and 7 in melt inclusion B yield a reproducibility better than 0.3‰
305 (2SD) (Table DR2). Also, multiple measurements (n = 75) located at the edge or in the center
306 of the olivine grain ARP73-10-03_16, which shows the largest topographical variation, yield
307 data clustering within 0.45‰ (2SD; Table DR3), comparable to the reproducibility obtained
308 during the same session for San Carlos reference material that has negligible topography
309 (0.40‰, 2SD). Moreover, $\delta^{18}O$ from melt inclusions within ARP73-10-03_16 A and B were
310 measured twice, in two different sessions and similar values were obtained. As the mount was
311 placed in the sample holder with a different orientation, this confirms that measured $\delta^{18}O$
312 variation cannot be due to sample topography or orientation. Based on these observation, we
313 find it highly unlikely that topography of the grains is responsible for the large variation of
314 $\delta^{18}O$ in the melt inclusions analyzed in this study. As the calibration of the SIMS analyses
315 reported here were made using several reference materials covering the range of melt
316 inclusions major elements (Fig. DR2). Hence we conclude that the observed $\delta^{18}O$ variations
317 are real in melt inclusions and do not represent analytical artefacts.

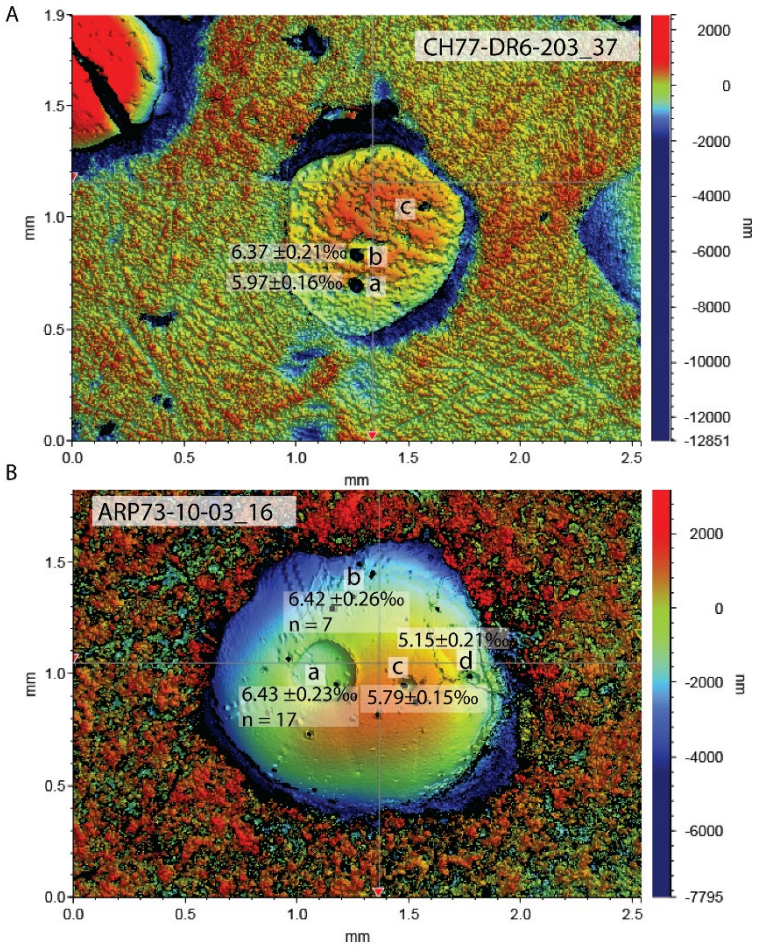

Figure 4: Example of profilometer images of the studied samples. A – ARP73-10-03_16 olivine; B – CH77-DR6-203_37 olivine. The number of points is specified when more than one analyses was obtained in the same inclusion, and the error (2SD) represents the reproducibility on the repeated measurements.

Effects of different magmatic processes

Partial melting causes large variations in the major- and trace- element concentrations of MORBs (e.g., Frey et al., 1993; Schilling et al., 1983; Zindler et al., 1979), but is not expected to largely fractionate oxygen isotopes. Indeed, Bindeman et al. (2012) estimate that extraction of 15% of the melt, assuming equilibrium is maintained throughout the melting, will change $\delta^{18}O$ by only 0.05‰. Even high degrees of partial melting (up to 42%) of a mantle source will

create less than 0.2 ‰ $\delta^{18}O$ variations (e.g. Eiler, 2001). Variation in the degree of partial melting will thus not be resolvable by SIMS, given the typical precision of ~0.3‰ 2SD. Hence, the lack of correlation between $\delta^{18}O$ and the abundance of incompatible elements such as $[La/Sm]_N$ for example (Figure 1), which are sensitive to degree of melting, indicates that variable extents of partial melting cannot explain the large $\delta^{18}O$ scatter measured in this study. Interestingly, ARP73-10-03 has a composition similar to that of typical MORB glass (N-MORB) in terms of $[La/Sm]_N$, K_2O and volatile contents, and average $\delta^{18}O$ composition (e.g., Eiler et al., 2000; Gale et al., 2013), whereas CH77-DR6-203 has higher $(La/Sm)_N$, volatiles, K_2O contents, and $\delta^{18}O$ than that of N-MORB glass (Figure 1). Differences in $(La/Sm)_N$, volatiles and K_2O contents between the two samples could reflect different degrees of melting, but the different average $\delta^{18}O$ rather suggests melting of an enriched mantle source for CH77-DR6-203. Despite the melting of different mantle sources for the two samples, resulting in different $\delta^{18}O$ for their respective melt inclusions, a similar variation of $\delta^{18}O$ (~2.5‰) is observed in melt inclusions for both samples.

The lack of correlation between $\delta^{18}O$ of the melt inclusions and the forsterite content of their host olivines do not support large fractionation of oxygen isotopes during magmatic evolution of the studied samples (Figure 5). This observation is consistent with an experimental study examining crystallization of a MORB melt dominated by olivine and plagioclase fractionation (Tormey et al., 1987), which shows that the oxygen isotopic composition of the melt should not vary by more than 0.1 ‰ for a MgO content between 3 to 8 wt% (Eiler, 2001). Recently, Bucholz et al. (2017) modelled change in $\delta^{18}O$ in tholeiite during fractional crystallization and also found minor change in $\delta^{18}O$ (up to 0.35‰ for composition comparable to ARP73-10-03 and CH77-203-DR3 melt inclusions).

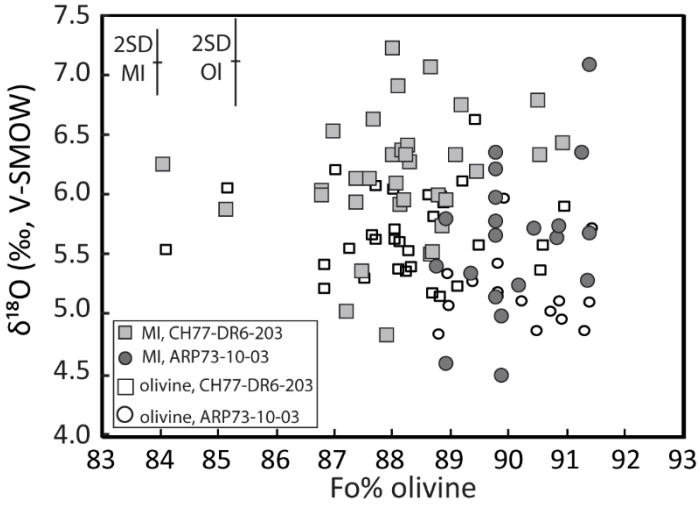

353

354 **Figure 5**: Plot of oxygen isotopes of olivine and of melt inclusions plotted against the Fo content of
355 the host olivines. Full symbols are for melt inclusions, empty symbols represent olivines.

356

357 Considering the low volatile concentrations in MORB lavas, the effect of magma degassing
358 on oxygen isotopes should be negligible. In fact, the total devolatilization of MORB magmas
359 will change the $\delta^{18}O$ by less than 0.1 ‰ (Eiler, 2001). Similarly, oxygen fugacity changes in
360 the magmatic system should not create any oxygen isotope ratio variations as the fractionation
361 of oxygen isotopes in the melt is not controlled by fO_2 (Lester et al., 2013).

362 Assimilation of altered oceanic (AOC) crust with variable $\delta^{18}O$ (1-6‰ for lower AOC and 7-
363 15‰ for upper AOC; e.g. Alt, 2003; Alt and Bach, 2006) may also affect the $\delta^{18}O$ variability
364 observed in melts (e.g., Genske et al., 2013). The assimilation process can be modeled by
365 simple mixing, because MORB melts and AOC have very similar oxygen concentrations. If
366 we consider a typical mantle composition of $\delta^{18}O$=5.5 ‰ (Eiler, 2001; Mattey et al., 1994)
367 and mix it with an altered upper oceanic crust with $\delta^{18}O$=15 ‰ (e.g., Alt, 2003), a minimum
368 of 17% assimilation of upper AOC is required to explain the highest $\delta^{18}O$ measured in melt
369 inclusions (7.1‰) from ARP73-10-03. This amount of upper AOC assimilation (>17%)
370 would, for example, result in Ba content of >62 ppm, assuming an average Ba content of the

upper AOC of 300 ppm (e.g., Kelley et al., 2003) and 13.9 ppm for uncontaminated MORB (Hofmann, 1988). As melt inclusions from ARP73-10-03 (N-MORB sample), have Ba contents typical of N-MORB (around 20 ppm; maximum 34 ppm Ba), we find that assimilation of upper crustal material is not likely to be responsible for the high $\delta^{18}O$ values measured in these melt inclusions. Similarly, a minimum of 22% assimilation of the upper AOC is required to obtain the lowest $\delta^{18}O$ (4.5‰) of the melt inclusions, assuming an extreme lower AOC composition of $\delta^{18}O$=1‰ (as in hydrothermal amphibolite veins; e.g., Alt and Bach, 2006). Assimilation of serpentinites that have $\delta^{18}O$ values of 2.0 to 6.7‰, with most of the values <5‰ (Barnes et al., 2014; Boschi et al., 2008) would require a larger amount of assimilation compared to AOC, and could not account for the $\delta^{18}O$ up to 7.1 ‰ or down to 4.5 ‰.

The absence of correlation between elements that are similarly incompatible in the dissolution reactions of pyroxene, plagioclase and spinel (e.g., S and Ce; Danyushevsky et al., 2004) suggests that local grain-scale dissolution-reaction mixing processes (Danyushevsky et al., 2004) is an unlikely process to explain the $\delta^{18}O$ variations in melt inclusions. In fact, open system local dissolution of minerals formed in equilibrium with a basaltic melt will not change the $\delta^{18}O$ composition of the ascending basaltic melt.

The $\delta^{18}O$ variability of 1.1 and 1.4 ‰ in the olivine crystals ($\delta^{18}O_{(Ol)}$) from ARP73-10-03 and CH77-DR6-203 (Table DR3), respectively, is an indicator that these olivine crystals record crystallization in a heterogeneous environment, or record a heterogeneous crystallization history. Considering the typical reproducibility of olivine measurements of 0.4‰, these variations are not likely to reflect analytical artefacts and should therefore represent real heterogeneities. In fact, individual crystals are homogeneous within measurement uncertainty of ca. 0.4 ‰, while different crystals from the same sample are more variable. In terms of major elements, each crystal is homogeneous (with the exception of P heterogeneities in some

396 olivines; Manzini et al., 2017), but all olivines have different Fo contents (Table DR3).
397 Within each sample, no clear trend is observed between Fo content and average $\delta^{18}O_{(Ol)}$ (Fig.
398 5). At a given Fo content, $\delta^{18}O_{(Ol)}$ varies up to 0.9‰. This observation suggests that these
399 olivine crystals from both samples grew in slightly heterogeneous environments (~0.9-1‰
400 variation).

401

402 *Olivine-melt inclusion isotopic disequilibrium*

403 Equilibrium fractionation between olivine and melt ($\Delta^{18}O_{ol\text{-}melt}$) at 1250°C is -0.6 ‰, based on
404 Matthews et al. (1998), which is equivalent to twice the uncertainty of the measured
405 compositions. As mentioned above, $\Delta^{18}O$ variability in the studied melt inclusions is larger
406 than the heterogeneity of their host olivines. Only 42 and 46% of melt inclusions from
407 ARP_73-10-03 and CH77-203-DR6 are in equilibrium with their host (Figure 3). The
408 remaining melt inclusions have either lower or higher $\Delta^{18}O_{ol\text{-}melt}$ compared to the theoretical
409 equilibrium value at 1250°C. While the proportion of melt inclusions in equilibrium with their
410 host olivine is similar for both samples, the proportion of melt inclusions with higher versus
411 lower $\Delta^{18}O_{ol\text{-}melt}$ is different for each sample. In detail, within an olivine containing several
412 exposed melt inclusions, $\Delta^{18}O_{ol\text{-}melt}$ can vary significantly. No correlation is observed between
413 olivine-melt isotopic disequilibrium and Fo content of the host olivine, which indicates that
414 disequilibrium conditions could have prevailed at any time during the samples' magmatic
415 history. An important observation is that melt inclusions in equilibrium with their host
416 olivines do not show significant $\delta^{18}O$ variation (5.7±0.3‰ for ARP73-10-03 and 6.3±0.5‰
417 for CH77-203-DR6). Assuming equilibrium between olivine and melt, variations in
418 temperature throughout crystal growth could affect $\Delta^{18}O_{ol\text{-}melt}$. However, the large variation of
419 $\Delta^{18}O_{ol\text{-}melt}$ would require a large and unrealistic temperature range, from 700°C for the lowest
420 $\Delta^{18}O_{ol\text{-}melt}$ to >2500 °C for the positive $\Delta^{18}O_{ol\text{-}melt}$.

We propose that the measured $\Delta^{18}O_{ol\text{-}melt}$ variations instead indicate disequilibrium. Lower or higher $\Delta^{18}O_{ol\text{-}melt}$ compared to theoretical equilibrium require either a process able to shift the equilibrium toward both higher and lower values, or a combination of different processes. Oxygen diffusion along the moving interface between melt and crystal during crystal growth or after melt inclusion entrapment is a process capable of generating isotopic disequilibrium between melt inclusions and their host olivine. Rapid crystal growth can lead to a local disequilibrium in the growth media, creating boundary layers in which elements with the lowest diffusivity in the melt and/or lowest partition coefficients (e.g., S, Cl, P, Al) will concentrate. It has been demonstrated that this process can create melt inclusion compositions with different major elements (Faure and Schiano, 2005; Watson and Müller, 2009), volatiles (S, Cl) and/or P content (Baker, 2008) compared to the bulk melt composition. Oxygen is also a slow diffusing element in relatively dry melts, with ^{16}O diffusing faster than ^{18}O (e.g., Lesher, 2010); therefore, such a boundary layer should have a higher $\delta^{18}O$ composition than the melt in which the crystal in growing. Melt inclusions from ARP-73-10-03 have major, trace and volatile elements compositions similar to MORB, with no enrichment in Al, S, Cl or Ca; however, some melt inclusions within this sample do have higher P contents due to olivine dissolution near P-rich (fast growing) domains (Manzini et al., 2017). No significant difference in $\delta^{18}O_{(Ol)}$ between P-rich and P-poor domains within each olivine are observed (Figure DR2). Moreover, $\delta^{18}O_{(Ol)}$ compositions of the recrystallized olivine (P-depleted halo) are similar to those of the primary olivine (Figure 6A). Figure 6B shows the $\delta^{18}O$ of melt inclusions from both samples, as a function of their location (in primary olivine, or in recrystallized domains), based on phosphorus maps of the host olivines. No systematic shift in $\delta^{18}O$ as a function of the olivine domain in which the melt inclusion is trapped can be resolved. Also, isotopic disequilibrium can be found in melt inclusions trapped in olivine with or without P zoning (Table DR2), suggesting that the MI-Olivine $\delta^{18}O$ disequilibrium and

large $\delta^{18}O$ variations in melt inclusions are not related to initial rapid crystal growth creating P-rich domains, nor to the dissolution of P-rich olivine domains.

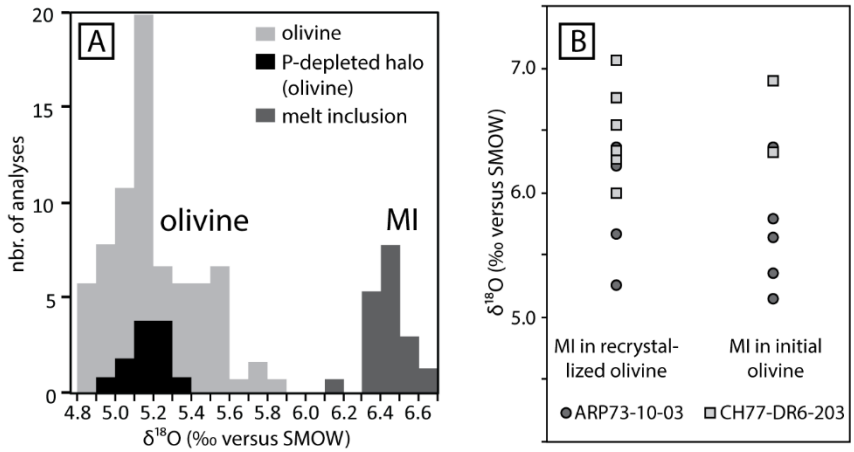

Figure 6: **A**: Comparison of $\delta^{18}O$ measured in the ARP73-10-03_16 olivine (P-enriched and P-normal zones), in the re-precipitated part (P-depleted zone around melt inclusion) and in the 2 melt inclusions situated in the P-zoned olivine part. No differences in oxygen isotope can be seen between the different parts of the olivine. **B**: Comparison of $\delta^{18}O$ measured in melt inclusions located in recrystallized olivine (i.e. close to a P-zoned region of the olivine) and in unzoned olivine parts, probably in initial olivine, that did not suffer from dissolution and re-precipitation. No differences can be observed between the two populations, but in general CH77-DR6-203 has higher $\delta^{18}O$ values than ARP73-10-03.

As argued above, olivine-hosted melt inclusions within the samples studied here suffered from PEC of olivine. Manzini et al. (2017) have shown that this thin (< 1 μm) layer crystallizes a few hours before eruption. This fast crystallization results in a strong P enrichment of the late-crystallized olivine. Post-entrapment crystallization could thus generate a thin boundary layer with a distinct (high) $\delta^{18}O_{(Ol)}$ composition and lower the initial $\delta^{18}O$ of the melt inclusions. Given the small volume of the PEC (1 μm layer compared to melt inclusion diameters of > 50 μm), it should not largely influence the melt inclusion

composition. This assumption is verified by the absence of a correlation between amount of PEC or P with $\delta^{18}O$ of the melt inclusions or $\Delta^{18}O_{ol\text{-}melt}$.

Diffusion of O in and out of the melt inclusions could in theory produce higher or lower $\Delta^{18}O_{ol\text{-}melt}$. Oxygen can diffuse as mono or multi-species. Indeed, O is present in CO_2 and H_2O molecules. It is known that water can diffuse in or out of melt inclusions (e.g., Chen et al., 2013; Gaetani et al., 2012; Portnyagin et al., 2008), but mostly in the form of H^+. Given the low water content involved in MORB systems, this should not produce large $\delta^{18}O$ variations in melt inclusions (Zhang and Ni, 2010). It is possible that CO_2 could largely degas in melt inclusion shrinkage bubbles (e.g., Moore et al., 2015); migration of CO_2 in the bubble may fractionate $\delta^{18}O$, but as ^{16}O is diffusing faster this could only generate higher $\delta^{18}O$. Melt inclusions with the lowest $\Delta^{18}O_{ol\text{-}melt}$ do not necessarily contain shrinkage bubbles, which indicates that fractionation of O isotopes is not related to shrinkage bubble formation.

Diffusion of O after melt inclusion entrapment would imply that melt inclusions were initially not in equilibrium with their host at the time of entrapment and thus cannot explain the origin of the large variation of $\delta^{18}O$ in the studied melt inclusions. If O isotopic diffusion occurred after melt inclusion entrapment, it should be limited based on the following observations: First, based on P profiles made from melt inclusions in olivines, melt inclusions were trapped for a few hours to a few days before quenching (Manzini et al., 2017). Using the diffusion data of Dohmen et al. (2002) (this dataset yields a diffusion coefficient of $\sim 9.3 \times 10^{12}$ in olivine at 1250°C), this amount of time would result in a small amount of O diffusing from melt inclusion to olivine over a profile no longer than 10 microns, which is not resolvable using the techniques employed in this study. This is confirmed by $\delta^{18}O$ profiles obtained from three different olivines, in which melt inclusions are either in disequilibrium (Figures 7A and DR2) or equilibrium (Figure 7B), starting at ~15-30µm from the inclusion wall, do not show any significant increase or decrease of $\delta^{18}O$ values toward the MI. Second, $\delta^{18}O$ profiles measured

within a single melt inclusion, from olivine wall to MI center, give similar values (Figure 8). Lastly, there is no correlation between the melt inclusion size and the $\delta^{18}O$ value of the melt inclusion.

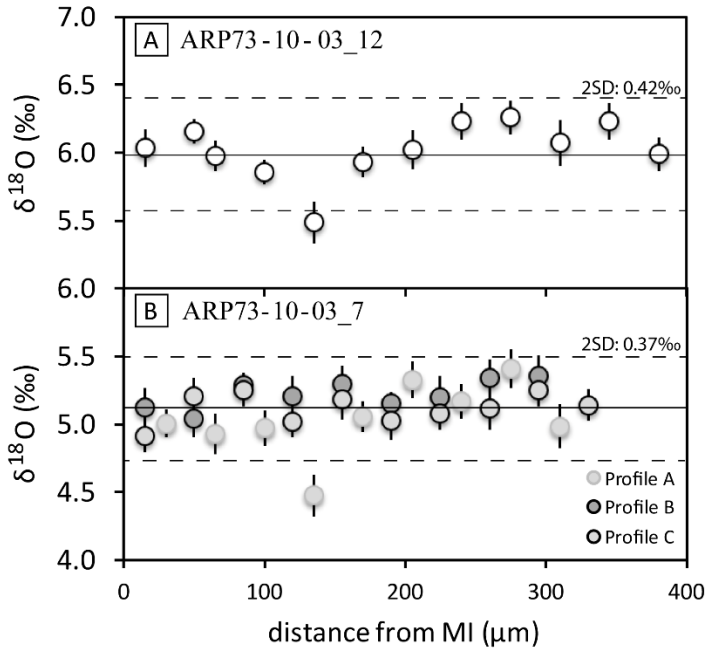

Figure 7: Oxygen isotopes profiles in olivines, starting from melt inclusion. A: oxygen isotopes profile in olivine ARP73-10-03_12, for which melt inclusion "a" is not in equilibrium. Profile starts from the melt inclusion. B: different $\delta^{18}O$ profiles done around the melt inclusion (in equilibrium) entrapped in olivine ARP-10-03_7. The 3 profiles start from 3 different locations around the melt inclusion and all are made in different directions. No clear diffusion profile from the melt inclusion toward the olivine can be observed. Black lines represent the average composition of olivine and dashed lines the 2 SD variations of the data along the profiles.

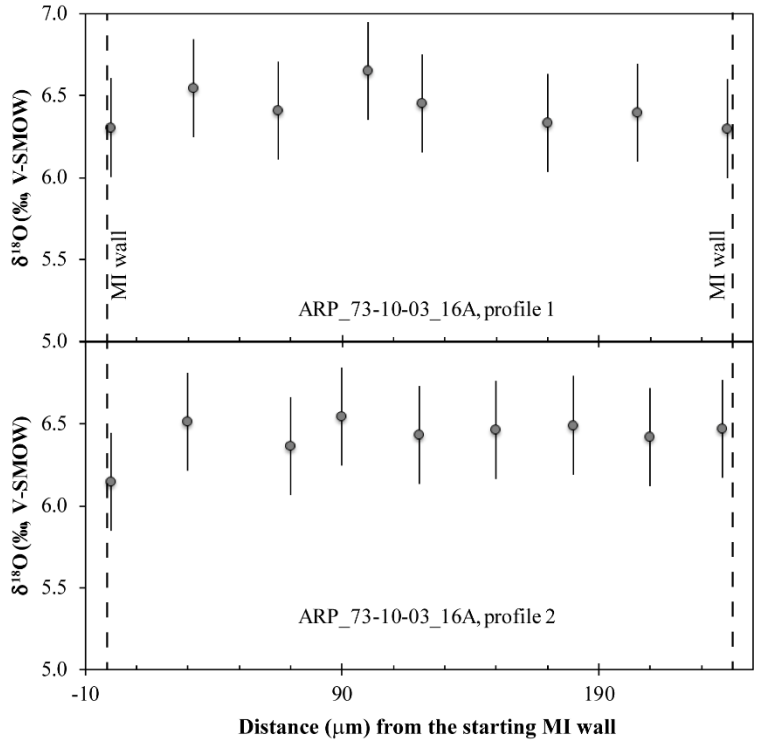

Figure 8: Oxygen isotopes profiles in melt inclusion APR-73-10-03_16A, from wall to wall. Two profiles were performed in this melt inclusion, perpendicular to one other.

In theory, oxygen diffusion could occur in response to a thermal gradient (Soret diffusion). Indeed, Kyser (1998) and Bindeman et al. (2013) reported significant isotopic fractionation of oxygen isotopes (up to 5.0‰) in anhydrous basaltic melt due to thermal diffusion, with migration of ^{18}O towards the colder regions. However, such a process has never convincingly been demonstrated in natural samples. Kyser (1998) pointed out that, even if thermally induced diffusion can lead to large $\delta^{18}O$ fractionation, the rapid decay of thermal gradient (< 10 days for 100° gradient at 1 cm from contact) makes it an unlikely process to happen in natural samples. Given the short timescale associated with the olivine residence time and melt inclusion formation in our samples (Manzini et al., 2017), a locally large thermal gradient (> 250°C) between migrating magma and conduit walls might be sustained before melt inclusion trapping. Assuming such a scenario, melt inclusions with $\delta^{18}O$ lower might form in olivine

517 located in the center of a conduit, whereas melt inclusions with higher $\delta^{18}O$ would form close
518 to the walls of the conduit; however, olivine crystallizing around the melt inclusions should
519 also have variable $\delta^{18}O$, which is not observed. This observation indicates that O diffusion in
520 response to a thermal gradient is not responsible for the $\delta^{18}O$ variation in melt inclusions.

521

522 ## Concluding remarks

523 The large variations (up to 2.5‰) observed in oxygen isotope ratios within melt inclusions
524 from 2 different Atlantic MORB samples (N-MORB and E-MORB) are not correlated with
525 major, trace or volatile elements. Oxygen isotope compositions of host olivines suggest a
526 small (<1‰) source heterogeneity for each sample. Less than half of the melt inclusions from
527 each sample are in isotopic equilibrium with their host olivines. The remaining melt
528 inclusions have either lower or higher isotopic fractionation compare to theoretical
529 equilibrium values. Boundary layer entrapment will only shift $\delta^{18}O$ toward higher values, and
530 the present dataset does not support this hypothesis. Fractionation diffusion of O during CO_2
531 migration into the shrinkage bubble will shift $\delta^{18}O$ toward lower values, but no evidence of
532 this process has been found. Another process capable of generating $\delta^{18}O$ fractionation both
533 higher and lower than equilibrium values is O diffusion in due to the presence of a thermal
534 gradient before melt inclusion entrapment (i.e. Soret diffusion). Although this process could
535 explain the large $\delta^{18}O$ variation measured, it would imply that a large, unrealistic, thermal
536 gradient (> 250°C) is sustained during the formation of melt inclusions. In addition, the
537 olivine directly surrounding the melt inclusion should also have a different $\delta^{18}O$ in this
538 scenario, which we do not observe.

539 Despite the marked disequilibrium in a majority of melt inclusions, our data do not show any
540 significant O diffusion in or out the melt inclusions. This is due to the short residence time at

high temperature after melt inclusion entrapment and the relatively large spatial resolution of the SIMS (10-15 microns). The exact process responsible for the melt inclusion-host $\delta^{18}O$ disequilibrium is thus not yet fully understood. Nonetheless, we argue that this dataset clearly shows that melt inclusions do not necessarily record the $\delta^{18}O$ composition of the magma in which their host grew. Caution should thus be taken before interpreting $\delta^{18}O$ variation as source process, especially when not related to any other tracer of common magmatic processes.

Acknowledgements

We acknowledge funding by the KIP6 PCI to L. P. Baumgartner. C-J. de Hoog, E. Bloch and O. Müntener are thanked for the useful comments which significantly improved the manuscript. The authors are thankful L. Danyushevsky, and anonymous reviewer and the editor, C. Chauvel, for their helpful reviews and comments. E. F. Rose-Koga acknowledges financial support from the Centre National de la Recherche Scientifique (INSU-SYSTER) and from the Région Auvergne-Rhône-Alpes.

559

560 ## References

561 Alt, J.C., 2003. Stable isotopic composition of upper oceanic crust formed at a fast spreading ridge,
562 ODP Site 801. Geochemistry, Geophys. Geosystems 4, 1–11.
563 https://doi.org/10.1029/2002GC000400

564 Alt, J.C., Bach, W., 2006. Oxygen isotope composition of a section of lower oceanic crust, ODP Hole
565 735B. Geochemistry, Geophys. Geosystems 7. https://doi.org/10.1029/2006GC001385

566 Baker, D.R., 2008. The fidelity of melt inclusions as records of melt composition. Contrib. to Mineral.
567 Petrol. 156, 377–395. https://doi.org/10.1007/s00410-008-0291-3

568 Barnes, J.D., Beltrando, M., Lee, C.T.A., Cisneros, M., Loewy, S., Chin, E., 2014. Geochemistry of
569 Alpine serpentinites from rifting to subduction: A view across paleogeographic domains and
570 metamorphic grade. Chem. Geol. 389, 29–47. https://doi.org/10.1016/j.chemgeo.2014.09.012

571 Bindeman, I.N., Kamenetsky, V.S., Palandri, J., Vennemann, T., 2012. Hydrogen and oxygen isotope
572 behaviors during variable degrees of upper mantle melting: Example from the basaltic glasses
573 from Macquarie Island. Chem. Geol. 310–311, 126–136.
574 https://doi.org/10.1016/j.chemgeo.2012.03.031

575 Bindeman, I.N., Lundstrom, C.C., Bopp, C., Huang, F., 2013. Stable isotope fractionation by thermal
576 diffusion through partially molten wet and dry silicate rocks. Earth Planet. Sci. Lett. 365, 51–62.
577 https://doi.org/10.1016/j.epsl.2012.12.037

578 Boschi, C., Dini, A., Früh-Green, G.L., Kelley, D.S., 2008. Isotopic and element exchange during
579 serpentinization and metasomatism at the Atlantis Massif (MAR 30°N): Insights from B and Sr
580 isotope data. Geochim. Cosmochim. Acta 72, 1801–1823.
581 https://doi.org/10.1016/j.gca.2008.01.013

582 Bougault, H., Dmitriev, L., Schilling, J.G., Sobolev, A., Joron, J.L., Needham, H.D., 1988. Mantle
583 heterogeneity from trace elements: MAR triple junction near 14°N. Earth Planet. Sci. Lett. 88,

27–36. https://doi.org/10.1016/0012-821X(88)90043-X

Bucholz, C.E., Jagoutz, O., VanTongeren, J.A., Setera, J., Wang, Z., 2017. Oxygen isotope trajectories of crystallizing melts: Insights from modeling and the plutonic record. Geochim. Cosmochim. Acta 207, 154–184. https://doi.org/10.1016/j.gca.2017.03.027

Chen, Y., Provost, A., Schiano, P., Cluzel, N., 2013. Magma ascent rate and initial water concentration inferred from diffusive water loss from olivine-hosted melt inclusions. Contrib. to Mineral. Petrol. 165, 525–541. https://doi.org/10.1007/s00410-012-0821-x

Cottrell, E., Spiegelman, M., Langmuir, C.H., 2002. Consequences of diffusive reequilibration for the interpretation of melt inclusions. New York 3.

Danyushevsky, L. V., Della-Pasqua, F.N., Sokolov, S., 2000a. Re-equilibration of melt inclusions trapped by magnesian olivine phenocrysts from subduction-related magmas: Petrological implications. Contrib. to Mineral. Petrol. 138, 68–83. https://doi.org/10.1007/PL00007664

Danyushevsky, L. V., Eggins, S.M., Falloon, T.J., Christie, D.M., 2000b. H_2O abundance in depleted to moderately enriched mid-ocean ridge magmas; Part I: Incompatible behaviour, implications for mantle storage, and origin of regional variations. J. Petrol. 41, 1329–1364. https://doi.org/10.1093/petrology/41.8.1329

Danyushevsky, L. V., Leslie, R.A.J., Crawford, A.J., Durance, P., 2004. Melt inclusions in primitive olivine phenocrysts: The role of localized reaction processes in the origin of anomalous compositions. J. Petrol. https://doi.org/10.1093/petrology/egh080

Danyushevsky, L. V., Plechov, P., 2011. Petrolog3: Integrated software for modeling crystallization processes. Geochemistry, Geophys. Geosystems 12. https://doi.org/10.1029/2011GC003516

Dohmen, R., Chakraborty, S., Becker, H.-W., 2002. Si and O diffusion in olivine and implications for characterizing plastic flow in the mantle. Geophys. Res. Lett. 29, 2030. https://doi.org/10.1029/2002GL015480

Dosso, L., Bougault, H., 1986. A hot spot at 14 N on the Mid-Atlantic Ridge: Isotopic (Sr, Nd) and trace element data. Eos Trans. AGU 67, 410.

610 Eiler, J.M., 2001. Oxygen Isotope Variations of Basaltic Lavas and Upper Mantle Rocks. Rev.
611 Mineral. Geochemistry 43, 319–364. https://doi.org/10.2138/gsrmg.43.1.319

612 Eiler, J.M., Schiano, P., Kitchen, N., Stolper, E.M., 2000. Oxygen-isotope evidence for recycled crust
613 in the sources of mid-ocean-ridge basalts. Nature 403, 530–534.

614 Faure, F., Schiano, P., 2005. Experimental investigation of equilibration conditions during forsterite
615 growth and melt inclusion formation. Earth Planet. Sci. Lett. 236, 882–898.
616 https://doi.org/10.1016/j.epsl.2005.04.050

617 Frey, F.A., Walker, N., Stakes, D., Hart, S.R., Nielsen, R., 1993. Geochemical characteristics of
618 basaltic glasses from theamar andfamous axial valleys, Mid-Atlantic Ridge (36°–37°N):
619 Petrogenetic implications. Earth Planet. Sci. Lett. 115, 117–136. https://doi.org/10.1016/0012-
620 821X(93)90217-W

621 Gaetani, G. a., O'Leary, J. a., Shimizu, N., Bucholz, C.E., Newville, M., 2012. Rapid reequilibration
622 of H_2O and oxygen fugacity in olivine-hosted melt inclusions. Geology 40, 915–918.
623 https://doi.org/10.1130/G32992.1

624 Gale, A., Dalton, C.A., Langmuir, C.H., Su, Y., Schilling, J.-G., Dalton, C.A., Langmuir, C.H., Su, Y.,
625 Schilling, J., 2013. The mean composition of ocean ridge basalts. Geochem. Geophys. Geosyst
626 14, 489–518. https://doi.org/10.1029/2012GC004334

627 Garcia, M.O., Ito, E.M.I., Eiler, J.M., Pietruszka, A.J., 1998. Crustal Contamination of Kilauea
628 Volcano Magmas Revealed by Oxygen Isotope Analyses of Glass and Olivine from Puu Oo
629 Eruption Lavas 39, 803–817.

630 Genske, F.S., Beier, C., Haase, K.M., Turner, S.P., Krumm, S., Brandl, P.A., 2013. Oxygen isotopes
631 in the Azores islands: Crustal assimilation recorded in olivine. Geology 41, 491–494.
632 https://doi.org/10.1130/G33911.1

633 Gurenko, A.A., Bindeman, I.N., Chaussidon, M., 2011. Oxygen isotope heterogeneity of the mantle
634 beneath the Canary Islands: insights from olivine phenocrysts. Contrib. to Mineral. Petrol. 162,
635 349–363. https://doi.org/10.1007/s00410-010-0600-5

636 Gurenko, A.A., Chaussidon, M., 2002. Oxygen isotope variations in primitive tholeiites of Iceland :
637 evidence from a SIMS study of glass inclusions , olivine phenocrysts and pillow rim glasses.
638 Earth Planet. Sci. Lett. 205, 63–79.

639 Gurenko, A.A., Chaussidon, M., 1997. Boron concentrations and isotopic composition of the Icelandic
640 mantle: evidence from glass inclusions in olivine. Chem. Geol. 135, 21–34.

641 Gurenko, A.A., Chaussidon, M., 1995. Enriched and depleted primitive melts included in olivine from
642 Icelandic tholeiites: origin by continuous melting of a single mantle column. Geochim.
643 Cosmochim. Acta 59, 2905–2917. https://doi.org/10.1016/0016-7037(95)00184-0

644 Harmon, R.S., Hoefs, J., 1995. Oxygen isotope heterogeneity of the mantle deduced from global 18O
645 systematics of basalts from different geotectonic settings. Contrib. to Mineral. Petrol. 95–114.

646 Hartley, M.E., Thordarson, T., Fitton, J.G., 2013a. Oxygen isotopes in melt inclusions and glasses
647 from the Askja volcanic system, North Iceland. Geochim. Cosmochim. Acta 123, 55–73.
648 https://doi.org/10.1016/j.gca.2013.09.008

649 Hartley, M.E., Thordarson, T., Fitton, J.G., 2013b. Oxygen isotopes in melt inclusions and glasses
650 from the Askja volcanic system, North Iceland. Geochim. Cosmochim. Acta 123, 55–73.
651 https://doi.org/10.1016/j.gca.2013.09.008

652 Hartley, M.E., Thordarson, T., Taylor, C., Fitton, J.G., EIMF, 2012. Evaluation of the effects of
653 composition on instrumental mass fractionation during SIMS oxygen isotope analyses of glasses.
654 Chem. Geol. 334, 312–323. https://doi.org/10.1016/j.chemgeo.2012.10.027

655 Helo, C., Longpré, M.A., Shimizu, N., Clague, D.A., Stix, J., 2011. Explosive eruptions at mid-ocean
656 ridges driven by CO 2-rich magmas. Nat. Geosci. 4, 260–263. https://doi.org/10.1038/ngeo1104

657 Hofmann, A.W., 1988. Chemical differentiation of the Earth : the relationship between mantle ,
658 continental crust , and oceanic crust 90, 297–314.

659 Jambon, A., Déruelle, B., Dreibus, G., Pineau, F., 1995. Chlorine and bromine abundance in MORB:
660 the contrasting behaviour of the Mid-Atlantic Ridge and East Pacific Rise and implications for
661 chlorine geodynamic cycle. Chem. Geol. 126, 101–117. https://doi.org/10.1016/0009-

2541(95)00112-4

Javoy, M., Pineau, F., 1991. The volatiles record of a “popping” rock from the Mid-Atlantic Ridge at 14°N: chemical and isotopic composition of gas trapped in the vesicles. Earth Planet. Sci. Lett. 107, 598–611. https://doi.org/10.1016/0012-821X(91)90104-P

Jin, Z.-M., Green, H.W., Zhou, Y., 1994. Melt topology in partially molten mantle peridotite during ductile deformation. Nature 372, 164.

Jochum, K.P., Stoll, B., Herwig, K., Willbold, M., Hofmann, A.W., Amini, M., Aarburg, S., Abouchami, W., Hellebrand, E., Mocek, B., Raczek, I., Stracke, A., Alard, O., Bouman, C., Becker, S., Dücking, M., Brätz, H., Klemd, R., de Bruin, D., Canil, D., Cornell, D., de Hoog, C.-J., Dalpé, C., Danyushevsky, L., Eisenhauer, A., Gao, Y., Snow, J.E., Groschopf, N., Günther, D., Latkoczy, C., Guillong, M., Hauri, E.H., Höfer, H.E., Lahaye, Y., Horz, K., Jacob, D.E., Kasemann, S.A., Kent, A.J.R., Ludwig, T., Zack, T., Mason, P.R.D., Meixner, A., Rosner, M., Misawa, K., Nash, B.P., Pfänder, J., Premo, W.R., Sun, W.D., Tiepolo, M., Vannucci, R., Vennemann, T., Wayne, D., Woodhead, J.D., 2006. MPI-DING reference glasses for in situ microanalysis: New reference values for element concentrations and isotope ratios. Geochemistry, Geophys. Geosystems 7, n/a-n/a. https://doi.org/10.1029/2005GC001060

Kamenetsky, V.S., Gurenko, A.A., 2007. Cryptic crustal contamination of MORB primitive melts recorded in olivine-hosted glass and mineral inclusions. Contrib. to Mineral. Petrol. 153, 465–481. https://doi.org/10.1007/s00410-006-0160-x

Kelley, K. a., Plank, T., Ludden, J., Staudigel, H., 2003. Composition of altered oceanic crust at ODP Sites 801 and 1149. Geochemistry, Geophys. Geosystems 4, n/a-n/a. https://doi.org/10.1029/2002GC000435

Kempton, P.D., Hawkesworth, C.J., Fowler, M., 1991. Geochemistry and isotopic composition of gabbros from layer 3 of the Indian Ocean crust, Hole 735B. Proc., Sci. results, ODP, Leg 118, Fract. Zo. Drill. Southwest Indian Ridge 127–143. https://doi.org/10.2973/odp.proc.sr.118.118.1991

688 Kent, A.J.R., 2008. Melt Inclusions in Basaltic and Related Volcanic Rocks. Rev. Mineral.
689 Geochemistry 69, 273–331. https://doi.org/10.2138/rmg.2008.69.8

690 Kita, N.T., Ushikubo, T., Fu, B., Valley, J.W., 2009. High precision SIMS oxygen isotope analysis
691 and the effect of sample topography. Chem. Geol. 264, 43–57.
692 https://doi.org/10.1016/j.chemgeo.2009.02.012

693 Kyser, T.K., Lesher, C.E., Walker, D., 1998. The effects of liquid immiscibility and thermal diffusion
694 on oxygen isotopes in silicate liquids. Contrib. to Mineral. Petrol. 133, 373–381.
695 https://doi.org/10.1007/s004100050459

696 Laubier, M., Gale, A., Langmuir, C.H., 2012. Melting and crustal processes at the FAMOUS segment
697 (mid-atlantic ridge): New insights from olivine-hosted melt inclusions from multiple samples. J.
698 Petrol. 53, 665–698. https://doi.org/10.1093/petrology/egr075

699 Laubier, M., Schiano, P., Doucelance, R., Ottolini, L., Laporte, D., 2007. Olivine-hosted melt
700 inclusions and melting processes beneath the FAMOUS zone (Mid-Atlantic Ridge). Chem. Geol.
701 240, 129–150. https://doi.org/10.1016/j.chemgeo.2007.02.002

702 Lecuyer, C., Reynard, B., 1996. High-temperature alteration of oceanic gabbros by seawater (Hess
703 Deep, Ocean Drilling Program Leg 147): Evidence from oxygen isotopes and elemental fluxes. J.
704 Geophys. Res. 101, 15883–15897.

705 Lesher, C.E., 2010. Self-diffusion in Silicate Melts: Theory, Observations and Applications to
706 Magmatic Systems. Rev. Mineral. Geochemistry 72, 269–309.
707 https://doi.org/10.2138/rmg.2010.72.7

708 Lester, G.W., Kyser, T.K., Clark, A.H., 2013. Oxygen isotope partitioning between immiscible silicate
709 melts with H_2O, P and S. Geochim. Cosmochim. Acta 109, 306–311.
710 https://doi.org/10.1016/j.gca.2013.01.037

711 Magenheim, A.J., Spivack, A.J., Michael, P.J., Gieskes, J.M., 1995. Chlorine stable isotope
712 composition of the oceanic crust: Implications for Earth's distribution of chlorine. Earth Planet.
713 Sci. Lett. 131, 427–432. https://doi.org/10.1016/0012-821X(95)00017-7

714 Manzini, M., Bouvier, A.S., Baumgartner, L.P., Müntener, O., Rose-Koga, E.F., Schiano, P., Escrig,
715 S., Meibom, A., Shimizu, N., 2017. Weekly to monthly time scale of melt inclusion entrapment
716 prior to eruption recorded by phosphorus distribution in olivine from mid-ocean ridges. Geology
717 45, 1059–1062. https://doi.org/10.1130/G39463.1

718 Mattey, D., Lowry, D., Macpherson, C., 1994. Oxygen isotope compositions of mantle peridotite.
719 Earth Planet. Sci. Lett. 128, 231–241.

720 Matthews, A., Stolper, E.M., Eiler, Epstein, S., 1998. Oxygen isotope fractionation among melts,
721 minerals and rocks. Goldschmidt Conf. Toulouse 971–972.

722 McDonough, W.F., Sun, S. -s., 1995. The composition of the Earth. Chem. Geol. 120, 223–253.
723 https://doi.org/10.1016/0009-2541(94)00140-4

724 McKenzie, D.P., 1984. The generation and compaction of partial melts. J. Petrol. 25, 713–765.
725 https://doi.org/https://doi.org/10.1093/petrology/25.3.713

726 Moore, L.R., Gazel, E., Tuohy, R., Lloyd, A.S., Esposito, R., Steele-MacInnis, M., Hauri, E.H.,
727 Wallace, P.J., Plank, T., Bodnar, R.J., 2015. Bubbles matter: An assessment of the contribution
728 of vapor bubbles to melt inclusion volatile budgets. Am. Mineral. 100, 806–823.

729 Naumov, V.B., Dorofeeva, V.A., Girnis, A. V., Yarmolyuk, V. V., 2014. Comparison of major,
730 volatile, and trace element contents in the melts of mid-ocean ridges on the basis of data on
731 inclusions in minerals and quenched glasses of rocks. Geochemistry Int. 52, 347–364.
732 https://doi.org/10.1134/S0016702914050073

733 Nielsen, R.L., Sours-Page, R.E., Harpp, K.S., 2000. Role of a Cl-bearing flux in the origin of depleted
734 ocean floor magmas. Geochemistry, Geophys. Geosystems 1.
735 https://doi.org/10.1029/1999GC000017

736 Peres, P., Kita, N.T., Valley, J.W., Fernandes, F., Schuhmacher, M., 2013. New sample holder
737 geometry for high precision isotope analyses. Surf. Interface Anal. 45, 553–556.
738 https://doi.org/10.1002/sia.5061

739 Portnyagin, M., Almeev, R., Matveev, S., Holtz, F., 2008. Experimental evidence for rapid water

740 exchange between melt inclusions in olivine and host magma. Earth Planet. Sci. Lett. 272, 541–
741 552. https://doi.org/10.1016/j.epsl.2008.05.020

742 Schiano, P., 2003. Primitive mantle magmas recorded as silicate melt inclusions in igneous minerals.
743 Earth-Science Rev. 63, 121–144. https://doi.org/10.1016/S0012-8252(03)00034-5

744 Schilling, J.G., Zajac, M., Evans, R., Johnston, T., White, W., Devine, J.D., Kingsley, R., 1983.
745 Petrologic and geochemical variations along the Mid-Atlantic Ridge from 29 degrees N to 73
746 degrees N. Am. J. Sci. 283, 510–586. https://doi.org/10.2475/ajs.283.6.510

747 Seitz, S., Baumgartner, L.P., Bouvier, A.S., Putlitz, B., Vennemann, T., 2017. Quartz Reference
748 Materials for Oxygen Isotope Analysis by SIMS. Geostand. Geoanalytical Res. 41, 69–75.
749 https://doi.org/10.1111/ggr.12133

750 Shimizu, N., 1998. The geochemistry of olivine-hosted melt inclusions in a FAMOUS basalt ALV
751 519-4-1. Phys. Earth Planet. Inter. 107, 183–201. https://doi.org/10.1016/S0031-9201(97)00133-
752 7

753 Sobolev, A. V., Shimizu, N., 1993. Ultra-depleted primary melt in an olivine fron the Mid-Atlantic
754 Ridge. Nature 363, 151–154.

755 Stakes, D.S., 1991. Oxygen and hydrogen isotope compositions of oceanic plutonic rocks: High-
756 temperature deformation and metamorphism of oceanic layer 3. Stable Isot. Geochemistry A
757 Tribut. to Samuel Epstein 77–90.

758 Tormey, D.R., Grove, T.L., Bryan, W.B., 1987. Experimental petrology of N-MORB near the Kane
759 Fracture Zone: 22-25°N, mid-Atlantic ridge. Contrib. Miner. Pet. 96, 121–139.

760 Van Orman, J.A., Grove, T.L., Shimizu, N., 2002. Diffusive fractionation of trace elements during
761 production and transport of melt in Earth's upper mantle. Earth Planet. Sci. Lett. 198, 93–112.
762 https://doi.org/10.1016/S0012-821X(02)00492-2

763 Wallace, P., Carmichael, I.S.E., 1992. Sulfur in basaltic magmas. Geochim. Cosmochim. Acta 56,
764 1863–1874. https://doi.org/10.1016/0016-7037(92)90316-B

765 Watson, E.B., Müller, T., 2009. Non-equilibrium isotopic and elemental fractionation during
766 diffusion-controlled crystal growth under static and dynamic conditions. Chem. Geol. 267, 111–
767 124. https://doi.org/10.1016/j.chemgeo.2008.10.036

768 Zhang, Y., Ni, H., 2010. Diffusion of H, C, and O Components in Silicate Melts, in: Reviews in
769 Mineralogy and Geochemistry. Mineralogical Society of America, pp. 171–225.
770 https://doi.org/10.2138/rmg.2010.72.5

771 Zindler, A., Hart, S.R., Frey, F.A., Jakobsson, S.P., 1979. Nd and Sr isotope ratios and rare earth
772 element abundances in Reykjanes Peninsula basalts evidence for mantle heterogeneity beneath
773 Iceland. Earth Planet. Sci. Lett. 45, 249–262. https://doi.org/10.1016/0012-821X(79)90127-4

774

775

776

777 **Supplementary material:**

778 **Figure DR1**: Calibration line for IMF correction for oxygen isotope analyses in glasses and

779 olivine.

780 **Figure DR2**: P-elemental X-ray map of the ARP73-10-03_16 olivine

781 **Table DR1:** SIMS conditions

782 **Table DR2:** Major, trace, volatile, elements and $\delta^{18}O$ composition of melt inclusions

783 **Table DR3:** Oxygen isotopes in olivines

784